scientific reports

Check for updates

OPEN

Application of novel nanomagnetic metal–organic frameworks as a catalyst for the synthesis of new pyridines and 1,4-dihydropyridines via a cooperative vinylogous anomeric based oxidation

Hassan Sepehrmansourie[1], Mahmoud Zarei[1]✉, Mohammad Ali Zolfigol[1]✉, Saeed Babaee[1] & Sadegh Rostamnia[2,3]✉

Herein, a new magnetic metal–organic frameworks based on Fe_3O_4 (NMMOFs) with porous and high surface area materials were synthesized. Then, NMMOFs were characterized by FT-IR, XRD, SEM, elemental mapping, energy dispersive X-ray (EDS), TG, DTG, VSM, and N_2 adsorption–desorption isotherms (BET). Fe_3O_4@Co(BDC)-NH_2 as a magnetic porous catalyst was applied for synthesis of novel fused pyridines and 1,4-dihydropyridines with pyrazole and pyrimidine moieties as suitable drug candidates under ultrasonic irradiation. The significant advantages of the presented methodology are mild, facile workup, high yields, short reaction times, high thermal stability, and reusability of the described NMMOFs catalyst.

Catalysis under ultrasonic irradiation has been widely applied for the preparation of organic compounds and catalysis[1–3]. On the other hand, hybrid organic–inorganic catalysts such as metal–organic frameworks (MOFs) as a new class of porous materials have high attention in chemical processes. Porous and magnetic materials have been widely used in biotechnology, magnetic resonance imaging (MRI), catalysis, adsorption, gas separation, and purification, optics, drug delivery, etc.[4–6]. However, metal–organic frameworks (MOFs) are a widespread strategy for the expansion of new porous materials to reach with the higher surface area. By selecting a suitable plan, reactants and reaction conditions can be correctly controlled by the porosity and structure of desired materials[7–13]. Magnetic catalysts have been used for the synthesis of a good range of pharmaceutical and chemical compounds, due to their easy removal and convenient separation[14–16]. The reported catalysts can be easily isolated from the reaction mixture with an external magnetic field[17–19]. Therefore magnetic metal–organic frameworks (MMOFs) have been used for various purposes due to their exciting properties[20–23], such as high thermal stability and application at the hard reaction conditions[24–26]. The chemistry of magnetic metal–organic frameworks and their corresponding applications comprehensively have been reviewed[27–29].

Fused *N*-heterocycles compounds with pyrazole and pyridines have shown a broad spectrum of biological and agricultural activities such as antitumor, cardiotonic hepatoprotactive, antihypertensive, antibronchitic, and antifungal activity[30–33]. Therefore, research and develop the new strategy are necessary for the synthesis of pyridines with pyrazole moieties. Pyridine derivatives are the central core of natural products such as NADP, clivimine, kedarcidin, and promothiocin A (Fig. 1)[34].

[1]Department of Organic Chemistry, Faculty of Chemistry, Bu-Ali Sina University, 6517838683 Hamedan, Iran. [2]Organic and Nano Group (ONG), Department of Chemistry, Iran University of Science and Technology (IUST), PO Box, 16846-13114 Tehran, Iran. [3]Organic and Nano Group (ONG), Department of Chemistry, Faculty of Science, University of Maragheh, PO Box, 55181-83111 Maragheh, Iran. ✉email: mahmoud8103@yahoo.com; zolfi@basu.ac.ir; rostamnia@iust.ac.ir

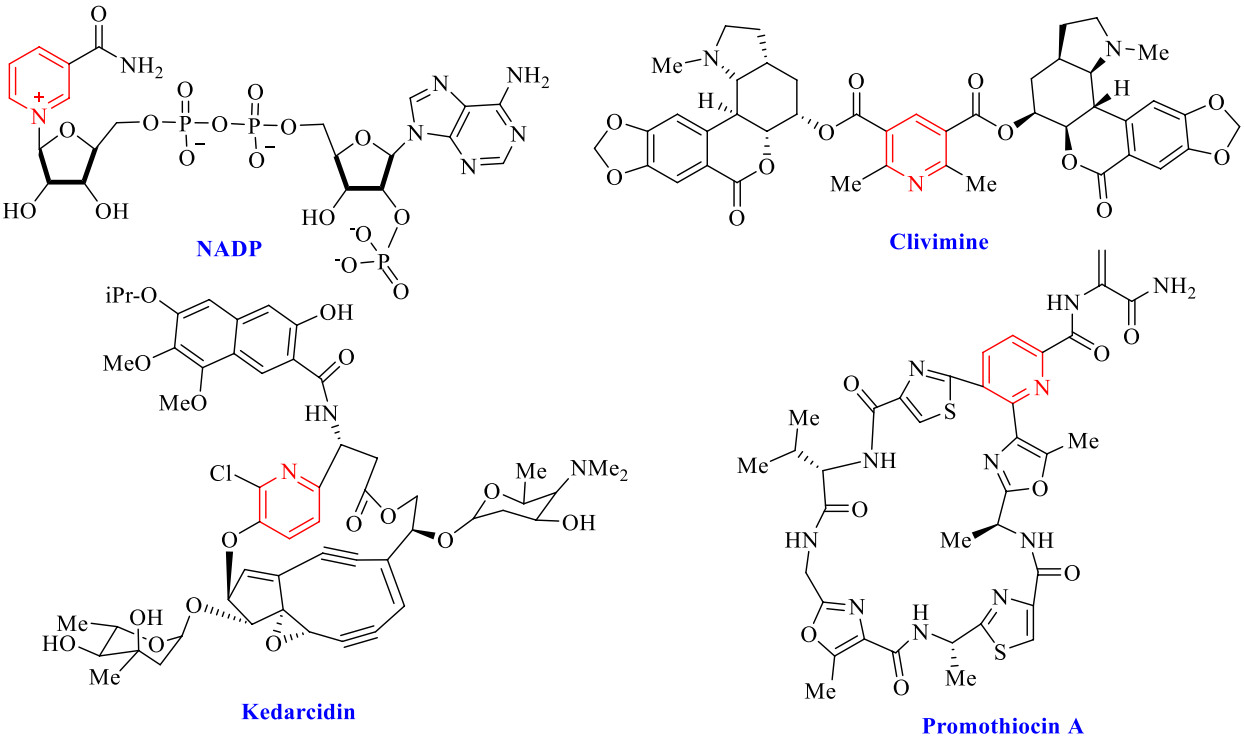

Figure 1. Structure of pyridine as natural products.

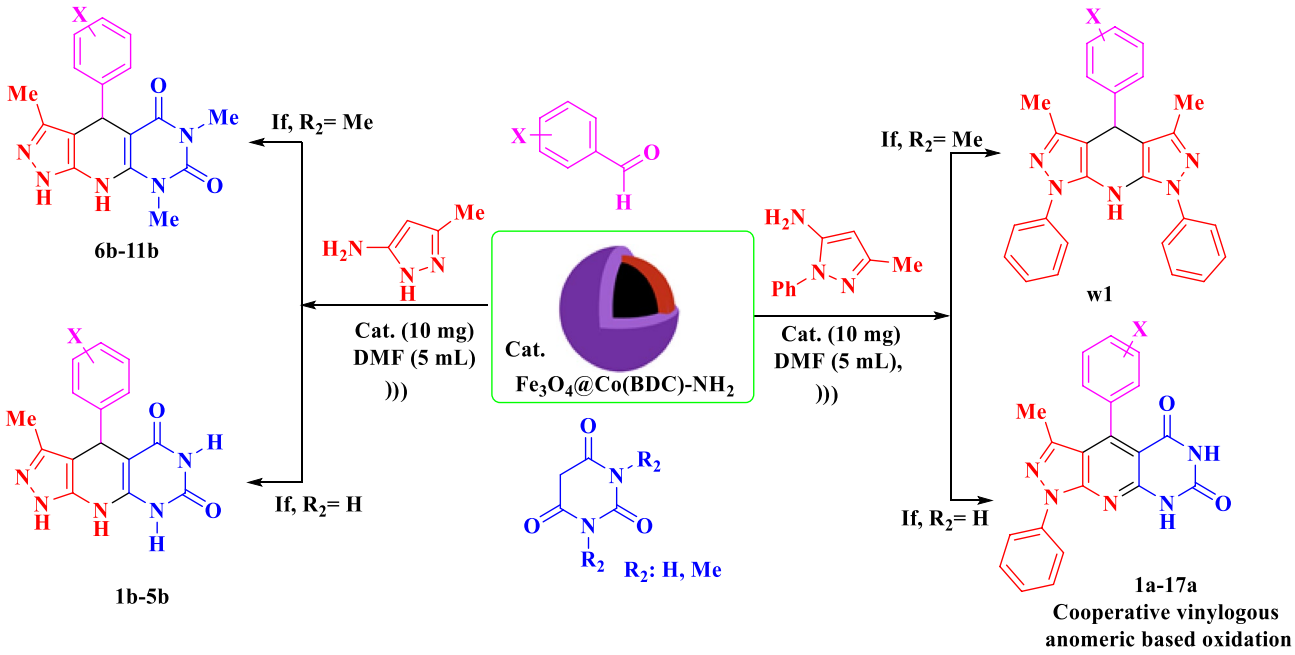

Scheme 1. Preparation of novel fused pyridines and 1,4-dihydropyridines with pyrazole and pyrimidine moieties by using Fe_3O_4@Co(BDC)-NH_2 as the catalyst.

Synthesis of composites of MOF and nano-magnetic Fe_3O_4 is our great research interest. With this aim, we have decided to synthesize nano-magnetic metal–organic frameworks Fe_3O_4@Co(BDC)-NH_2 as a porous and magnetic catalyst under ultrasonic irradiation condition. This nanomagnetic metal–organic frameworks (NMMOFs) was applied in the synthesis of novel fused pyridines and 1,4-dihydropyridines with pyrazole and pyrimidine moieties by using the corresponding precursors in DMF (5 mL) as solvent under ultrasonic irradiation (Scheme 1).

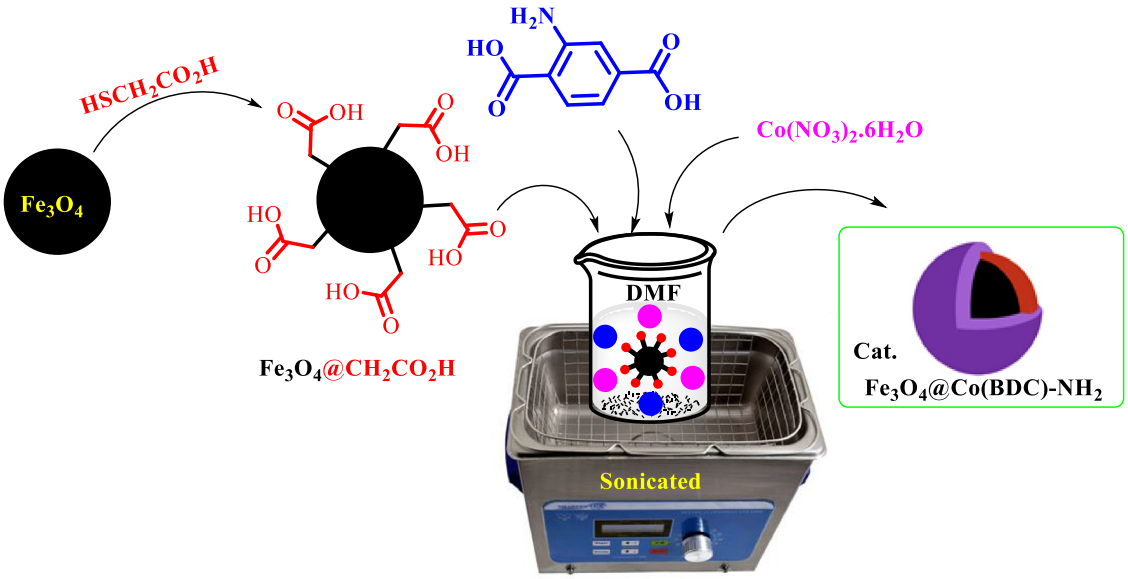

Scheme 2. Synthesis of Fe_3O_4@Co(BDC)-NH_2 as a nanomagnetic metal–organic frameworks.

Experimental

Materials and methods. All chemicals were purchased from Merck Chemical Company. The known products were identified by comparison of their melting points and spectral data with those reported in the literature. To scrutinize the progress of the reaction silica gel SIL G/UV 254 plates were used. From the model of the BRUKER Ultra shield, NMR spectrometer (δ in ppm) was recorded ^{1}H NMR (400 MHz) and ^{13}C NMR (100 MHz). Recorded on a Büchi B-545 apparatus in open capillary tubes were melting points. The PerkinElmer PE-1600-FTIR device was registered for the infrared spectra of compounds. SEM was performed using a scanning electron microscope for field publishing made by TE-SCAN. Thermal gravimetry (TG), differential thermal gravimetric (DTG) and differential thermal (DTA) were analyzed by a Perkin Elmer (Model: Pyris 1). The analysis 25–1000 °C, temperature increase rate of 10 °C min^{-1}.

General procedure for the synthesis of Fe_3O_4@CH_2CO_2H. Fe_3O_4 was prepared according to the previously reported literature[35,36]. Then, in a 25 mL round-bottomed flask, a mixture of Fe_3O_4 (1 g), $HSCH_2CO_2H$ (10.0 mmol, 1.38 g), and EtOH (30 mL) were added and refluxed for 24 h. After this time, a dark brown precipitate was appeared, which it is isolated by using a magnet. The obtained Fe_3O_4@CH_2CO_2H (1.95 g) was dried under vacuum[23].

General procedure for the synthesis of Fe_3O_4@Co(BDC)-NH_2. At first, a solution of 45.0 mM of $Co(NO_3)_2{\cdot}6H_2O$ (2.34 g in 180 mL DMF) (solution I) and 45.0 mM of H_2BDC-NH_2 (1.46 g in 180 mL DMF) (solution II) were prepared respectively. In a 25 mL glass vials, a mixture of Fe_3O_4@CH_2CO_2H (0.5 g) and 10 mL of solution I were sonicated for 20 min. Then, this mixture was separated by a permanent magnet and washed with DMF as step I. Then, a mixture of step I and 10 mL of solution II were sonicated for 45 min. The produced solid was separated by a permanent magnet and washed with EtOH as step II. In continued, two strategies (a mixture of step I and step II) were repeated 18 times, respectively. Finally, Fe_3O_4@Co(BDC)-NH_2 (0.8 g) was dried under vacuum for 2 h (Scheme 2).

General procedure for the synthesis of novel fused pyridines and 1,4-dihydropyridines. In a 10 mL round-bottomed, a mixture of aldehyde (1.0 mmol), pyrimidine (1,3-dimethylpyrimidine-2,4,6(1*H*,3*H*,5*H*)-trione or pyrimidine-2,4,6(1*H*,3*H*,5*H*)-trione) and pyrazole-5-amine (3-methyl-1*H*-pyrazole-5-amine or 3-methyl-1-phenyl-1*H*-pyrazole-5-amine) derivatives] and Fe_3O_4@Co(BDC)-NH_2 (10 mg) as a catalyst were mixed in DMF (5 mL) as solvent under ultrasonic irradiation. After completion of the reaction (monitor by TLC *n*-hexane/ethyl acetate; 4:6), the catalyst was separated by an external magnet. Finally, the mixture was poured into H_2O and filtered off its precipitate. The obtained residue was washed with warm ethanol and dried at 100 °C (Scheme 1).

Result and discussion

The systematic study of the stereoelectronic effects in target molecules, allows for the design of synthetic strategies based on a nomerically driven stereoselective reactions, or highly biased equilibria among isomeric products. To the best of our knowledge, many biological processes involve the oxidation–reduction of substrates by NAD^+/NADH, respectively[37–41]. The key feature of the oxidation mechanism is hydride transfer from carbon via stereoelectronic interactions. Thus the development of stereoelectronic effects leads to knowledge-based designing

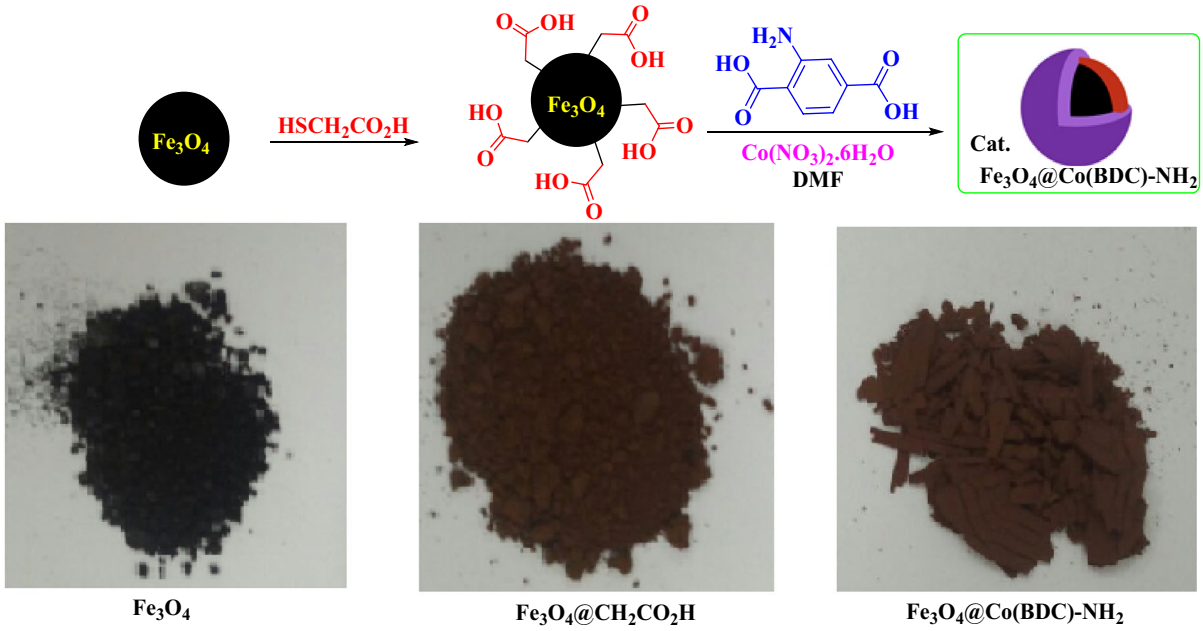

Figure 2. Stepwise synthesis of the nanomagnetic metal–organic frameworks (NMMOFs) system.

of biomimetic reactions. The obtained results from this research will be supporting the idea of rational designs, syntheses, and applications of tasked-specific catalysts and molecules for the development of stereoelectronic effects in the course of organic synthesis. With this aim, a nanomagnetic metal–organic frameworks (NMMOFs) was designed, characterized and applied for the preparation of pyridines fused with pyrazole and pyrimidine under ultrasonic irradiation.

At first, nanomagnetic metal–organic frameworks (NMMOFs) were synthesized (Scheme 2). Its schematic synthesis is showed in Fig. 2. The synthesized Fe_3O_4@Co(BDC)-NH_2 fully characterized by applying FT-IR, XRD, SEM, elemental mapping, energy dispersive X-ray (EDS), TG, DTG, VSM and N_2 adsorption–desorption isotherms (BET).

FT-IR spectrum of H_2BDC-NH_2, Fe_3O_4, Fe_3O_4@CH_2CO_2H, and Fe_3O_4@Co(BDC)-NH_2 are shown in Figure S1 (see supporting information). The absorption bands at 670 cm^{-1} linked to the stretching vibrational modes of Fe–O groups in Fe_3O_4. The absorption bands at 1741, 2924, and 3426 cm^{-1} related to C=O, C–H and, O–H stretching respectively in Fe_3O_4@CH_2CO_2H. Also, the absorption bands at 633 cm^{-1} and 3318–3448 cm^{-1} are related to Co–O and N–H_2 stretching respectively, of Fe_3O_4@Co(BDC)-NH_2. Finally, the differences between H_2BC-NH_2, Fe_3O_4, Fe_3O_4@CH_2CO_2H, and Fe_3O_4@Co(BDC)-NH_2 in the FT-IR spectrum were confirmed the synthesis of Fe_3O_4@Co(BDC)-NH_2.

The particle size and shape, as well as the morphology of Fe_3O_4@CH_2CO_2H, Fe_3O_4, MOF-Co(BDC)-NH_2, $Co(NO_3)_3{\cdot}6H_2O$ and Fe_3O_4@Co(BDC)-NH_2 were studied by XRD (Fig. 3), and SEM (Fig. 4). The comparison XRD pattern of JCPDS (red line), Fe_3O_4 (black line), $Co(NO_3)_3{\cdot}6H_2O$ (purple line), Simulated XRD (orange line), MOF-Co(BDC)-NH_2 (green line), Fe_3O_4@CH_2CO_2H (brown line) and Fe_3O_4@Co(BDC)-NH_2 (blue line) is assembled according to the liturture servey at the range of 5°–80° in Fig. 3[42]. The phase of Co oxide and Fe_3O_4 in Fe_3O_4@Co(BDC)-NH_2 as standard brown line (ICDD Card: 80-1540) of Co and pinks standard line (JCP2: 75-449) of Fe_3O_4 in the standard references. Also, Peaks of Fe_3O_4@Co(BDC)-NH_2 exhibited $2\theta = 18.3°$, 30.2°, 35.6°, 43.3°, 53.6°, 57.3°, 62.8° and 74.2° corresponding to diffraction lines (111), (220), (311), (400), (422), (511), (440) and (533). Then, the averaged interlunar distance and sizes of crystal were calculated by the Scherer equation and Bragg equation, which are determined 0.67 nm (single peak at 12.8 and 17.5–37.5 nm range (Table S1 see in supporting information)[43,44].

For comparison, structure and elementals in the synthesis of step by step Fe_3O_4@CH_2CO_2H and Fe_3O_4@Co(BDC)-NH_2 were also studied with energy dispersive X-ray analysis (EDX) analysis (Figure S2 see supporting information). The structures of Fe_3O_4@Co(BDC)-NH_2 and Fe_3O_4@CH_2CO_2H were verified with existence of Fe, Co, N, C, O and Fe, C, O, and S atoms respectively [45]. Then, elementals dispersed over the surface of the catalyst, and step Fe_3O_4@Co(BDC)-NH_2 was checked out by SEM-elemental mapping (Figure S3 see supporting information). The images in Figure S3 shows that all kinds of elements are well dispersed over the surface of Fe_3O_4@Co(BDC)-NH_2. The difference between EDX analysis and SEM-elemental mapping is confirmed by the structure of Fe_3O_4@Co(BDC)-NH_2.

In another investigation, the particle size and shape, as well as the morphology of Fe_3O_4@Co(BDC)-NH_2 were examined by scanning electron microscope (SEM) (Fig. 4). As shown in Fig. 4, nano-spherical particles of the nanomagnetic metal–organic frameworks (NMMOFs) are in the nanoscale, as the particles are quite overlapped with different crystallite size as observed in SEM Transmission electron microcopy (TEM) images of Fe_3O_4@Co(BDC)-NH_2 catalyst reveal that the particles shape is spherical and the particle size is up to 50 nm (Fig. 5).

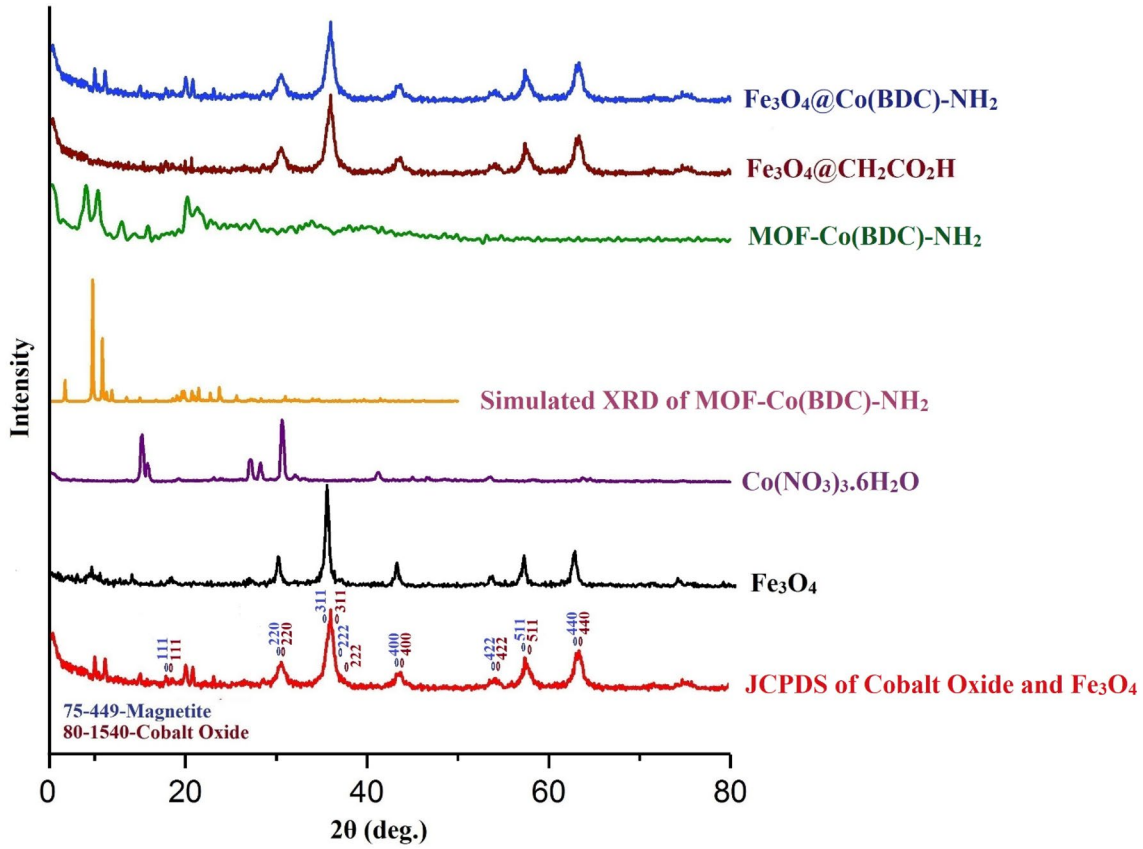

Figure 3. Comparison XRD pattern of JCPDS (red line), Fe_3O_4 (black line), $Co(NO_3)_3{\cdot}6H_2O$ (purple line), Simulated XRD (orange line), MOF-Co(BDC)-NH_2 (green line), Fe_3O_4@CH_2CO_2H (brown line) and Fe_3O_4@Co(BDC)-NH_2 (blue line).

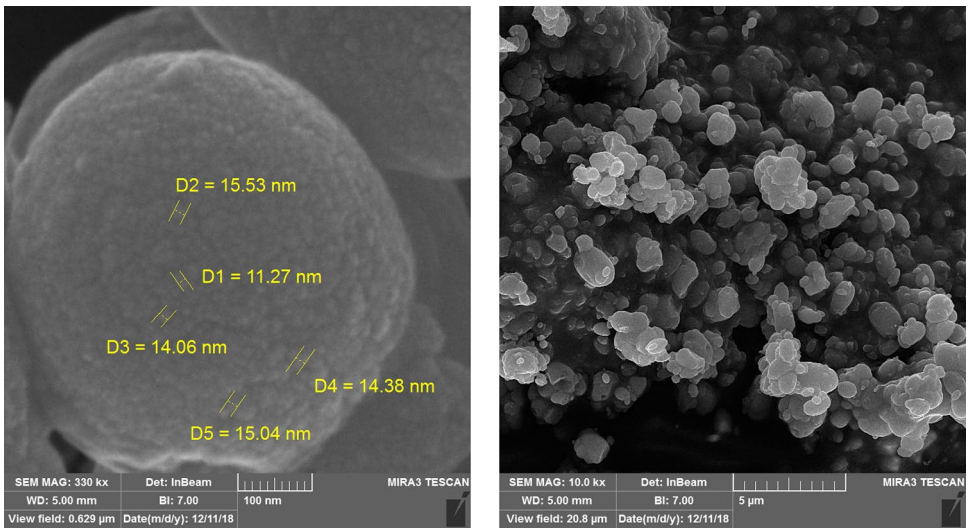

Figure 4. Scanning electron microscope (SEM) images of Fe_3O_4@Co(BDC)-NH_2.

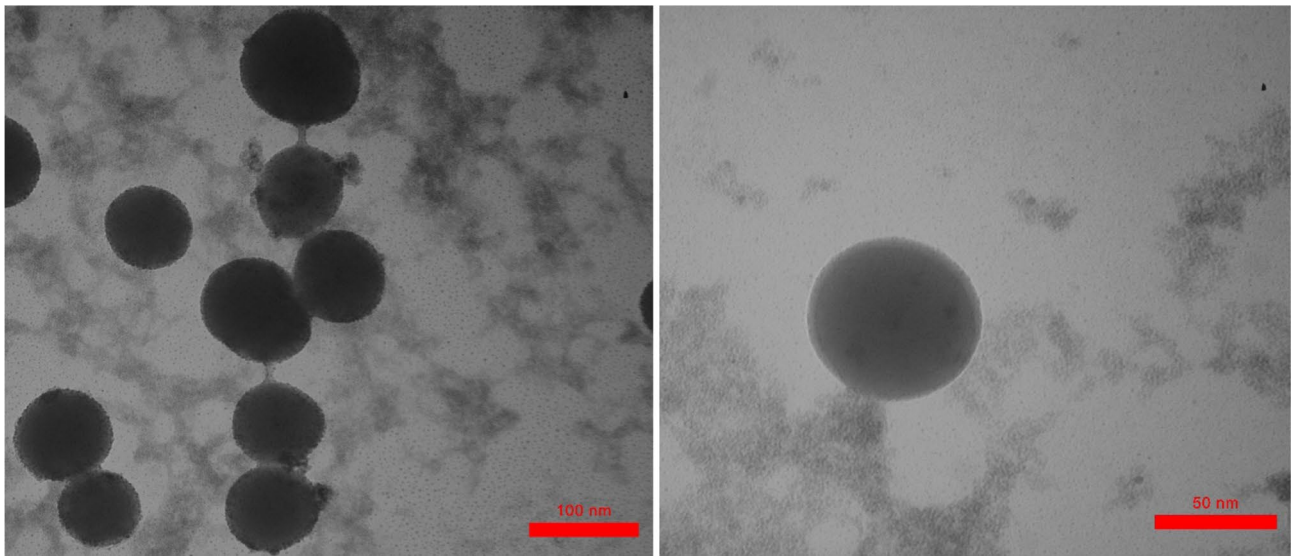

Figure 5. Transmission electron microscopy (TEM) images of Fe_3O_4@Co(BDC)-NH_2.

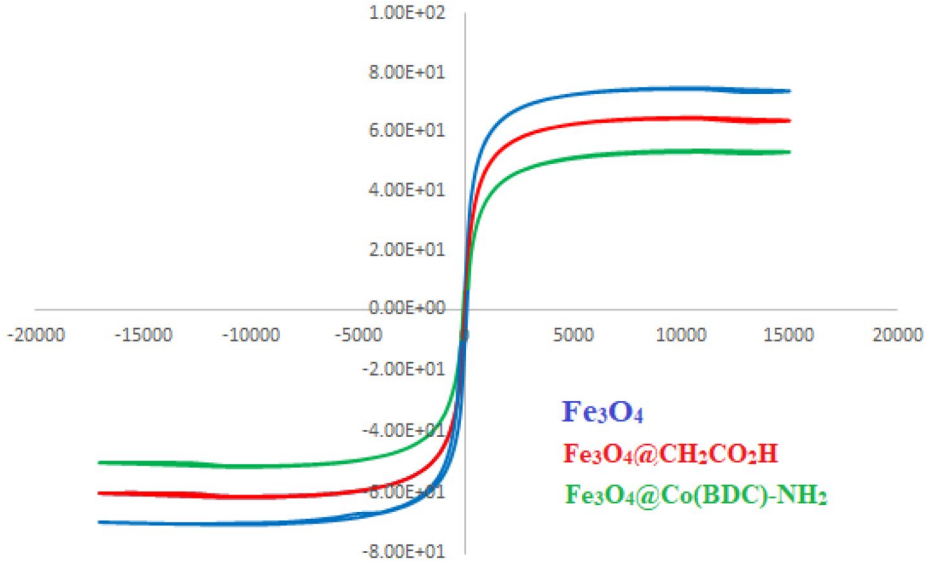

Figure 6. Vibrating sample magnetometer (VSM) of Fe_3O_4, Fe_3O_4@CH_2CO_2H, and Fe_3O_4@Co(BDC)-NH_2.

The magnetic measurement of Fe_3O_4, Fe_3O_4@CH_2CO_2H, and Fe_3O_4@Co(BDC)-NH_2 are shown in Fig. 6. Based on Fig. 6, the vibrating sample magnetometer (VSM) of Fe_3O_4, Fe_3O_4@CH_2CO_2H, and Fe_3O_4@Co(BDC)-NH_2 were examined and reduced from 64.4, 60.1 up to 54.3 μg^{-1} respectively. Therefore, these decreases are the result of coating with its corresponding layers.

In another investigation, the structural and thermal stability of Fe_3O_4@Co(BDC)-NH_2 was also determined using the technique of the thermal gravimetric (TG), derivative thermal gravimetric (DTG), as well as the differential thermal analysis (DTA) (Figure S4 see in supporting information). First stage weight loss is about 100 °C, associated with the removal of possible solvents (organic and water), which was used in the course of catalyst preparation. Then, twice a step of weight loss has occurred at about 300 °C, which is the onset of the structural degradation of the catalyst.

For the determination of surface structural parameters, the N_2 adsorption/desorption technique was used. The results of N_2 adsorption/desorption were plotted in Fig. 7. The obtained surface area based on BET isotherm is 22.35 $m^2\ g^{-1}$. The total pore volume of the catalyst is 0.02 $cm^3\ g^{-1}$. Also, for studying the textural properties of MOF-Co(BDC)-NH_2 the N_2 adsorption–desorption isotherms were used (Fig. 7). The adsorption isotherm is type III and the appearance of hysteresis loop shows the presence of mesopores in the sample. The calculated surface areas based on BET equation and total pore volumes are 86 $m^2\ g^{-1}$ and 0.36 $cm^3\ g^{-1}$ respectively. The pore size distribution of MOF-Co(BDC)-NH_2 based on BJH method is shown (Figure S5 see in supporting

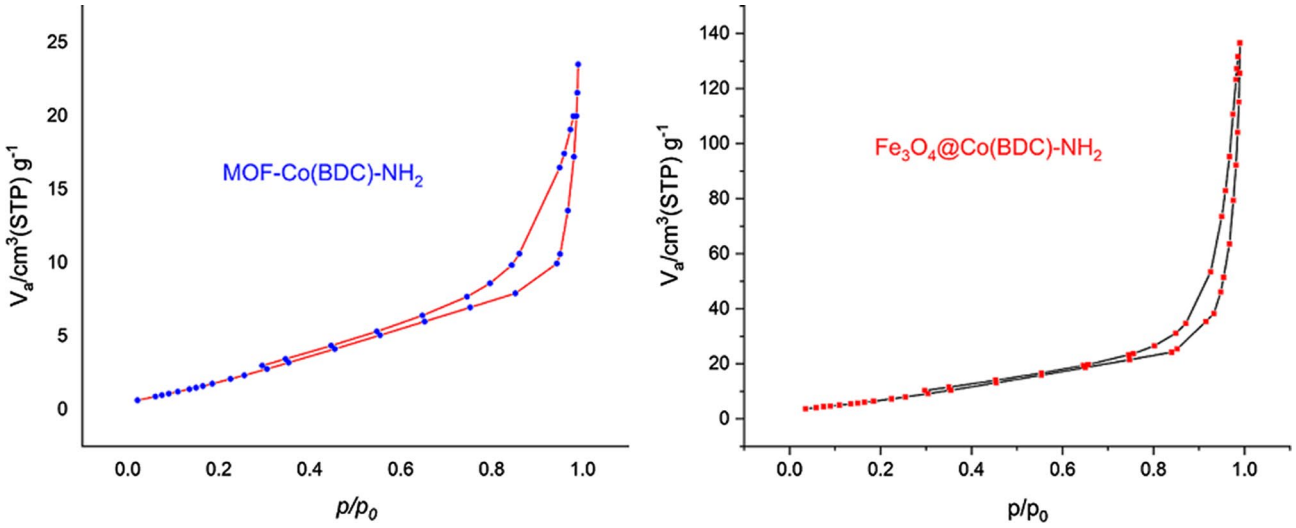

Figure 7. Nitrogen adsorption–desorption isotherm (BET) of Fe_3O_4@Co(BDC)-NH_2 and MOF-Co(BDC)-NH_2.

information). This plot clearly shows presence of micropores (size < 2 nm) and mesopores (2 < size < 50 nm) in the sample, however the micropores are more abundant.

After the synthesis and characterization of Fe_3O_4@Co(BDC)-NH_2, it was applied for the synthesis of novel mono, bis and tris novel fused pyridines and 1,4-dihydropyridines with pyrazole and pyrimidine moieties by using the corresponding precursors such as 3-methyl-1,4-diphenyl-1,8-dihydro-5*H*-pyrazolo[4′,3′:5,6]pyrido[2,3-*d*]pyrimidine-5,7(6*H*)-dione and 3-methyl-4-phenyl-1,4,8,9-tetrahydro-5*H*-pyrazolo[4′,3′:5,6]pyrido[2,3-*d*]pyrimidine-5,7(6*H*)-dione. The above mentioned products were obtained by reaction of 4-nitro benzaldehyde (1.0 mmol, 0.151 g), 3-methyl-1-phenyl-1*H*-pyrazole-5-amine (1.0 mmol, 0.174 g) and pyrimidine-2,4,6(1*H*,3*H*,5*H*)-trione (1.0 mmol, 0.128 g) as a model for the optimization the reaction conditions. The optimized data is listed in Table 1. As shown in Table 1, the best of choice for the synthesis of 3-methyl-1,4-diphenyl-1,8-dihydro-5*H*-pyrazolo[4′,3′:5,6]pyrido[2,3-*d*]pyrimidine-5,7(6*H*)-dione was achieved in the presence of 10 mg Fe_3O_4@Co(BDC)-NH_2 in DMF (5 mL) as solvent under ultrasonic irradiation (entry 4, Table 1). The model reaction was also studied by using several solvents such as H_2O, CH_3CN, *n*-hexane, $CHCl_3$, MeOH, EtOH, CH_2Cl_2, EtOAc (5 mL) and solvent-free condition in the presence of 10 mg of Fe_3O_4@Co(BDC)-NH_2. The results of the reaction did not improve (Table 1, entries 6–13). Also, the model reaction was also studied in the magnetic stirrer condition at room temperature under the solvent-free reaction (Table 1, entry 14).

After optimizing the reaction conditions, Fe_3O_4@Co(BDC)-NH_2(10 mg) is applied to synthesis a good range of novel biological and pharmacological candidate compounds using various aromatic aldehydes (trephetaldehyde, iso-trephetaldehyde, tris-aldehyde, bearing electron-donating and electron-withdrawing groups), pyrimidine (1,3-dimethylpyrimidine-2,4,6(1*H*,3*H*,5*H*)-trione, pyrimidine-2,4,6(1*H*,3*H*,5*H*)-trione) and pyrazole-5-amine (3-methyl-1*H*-pyrazole-5-amine, 3-methyl-1-phenyl-1*H*-pyrazole-5-amine) derivatives. As shown in Table 2, the obtained results indicated that Fe_3O_4@Co(BDC)-NH_2 is appropriate for the preparation of target molecules in high to excellent yields (65–90%) with in relatively short reaction times (20–40 min). Furthermore, the model reaction is tested by the reaction of 3-methyl-1*H*-pyrazole-5-amine, and 3-methyl-1*H*-pyrazole-5-amine to give a mixture of the corresponding pyridine and 1,4-dihydropyridine respectively.

In the proposed mechanism, the aldehyde is activated by Fe_3O_4@Co(BDC)-NH_2. In the initial step, intermediate (**I**) is produced by the reaction of pyrimidine (R_2 = H, Me) and activated aldehyde. In the next step, intermediate (**II**) is prepared with losing one molecule of H_2O. In the third step, pyrazole-5-amine (R_1 = H, Ph) derivatives react with intermediate (**II**) to gives intermediate (**IV**) after tautomerization. Then, intermediate (**IV**) gives intermediate (**V**) after intramolecular cyclization and losing another molecule of H_2O. In the last step, the lone pair electrons of N atoms of 1,4-dihydropyridine (**VI**) interacts through C–C double bonds with a vacant anti-bonding orbital of C–H bond ($n_N \rightarrow \sigma_{C-H}^*$ and $\pi_{C=C} \rightarrow \sigma_{C-H}^*$) and weaken it, so that is favoring for hydride transfer and H_2 releasing from intermediate **VI** to generate its corresponding pyridinium salt. The achieved data from the optimization of described reaction under argon and nitrogen atmospheres verified our suggestion for oxidation and aromatization of intermediate **VI**. On the other hand, 1,4-dihydropyridine (**VI**) is converted to its corresponding pyridinium intermediate (**VII**), via a cooperative vinylogous anomeric based oxidation and releasing a hydrogen molecule ($-H_2$)[47–55]. Finally, the desired pyridine fused with pyrazole and pyrimidine moiety (**B**) is obtained via removing a proton from the pyridinium intermediate (**VII**). When, 3-methyl-1*H*-pyrazole-5-amine was used instead of 3-methyl-1-phenyl-1*H*-pyrazole-5-amine after intramolecular cyclization and losing a molecule of water, intermediate (**VI**) is converted to product (**A**) (Scheme 3). Interestingly, the 1,4-dihydropyridines (**A**) did not convert to their corresponding pyridines.

The reusability of Fe_3O_4@Co(BDC)-NH_2 was also investigated. The reaction of 4-nitro benzaldehyde (1.0 mmol, 0.151 g), 3-methyl-1-phenyl-1*H*-pyrazole-5-amine (1.0 mmol, 0.174 g) and pyrimidine-2,4,6(1*H*,3*H*,5*H*)-trione (1.0 mmol, 0.128 g) was selected as a model reaction under ultrasonic irradiation. The

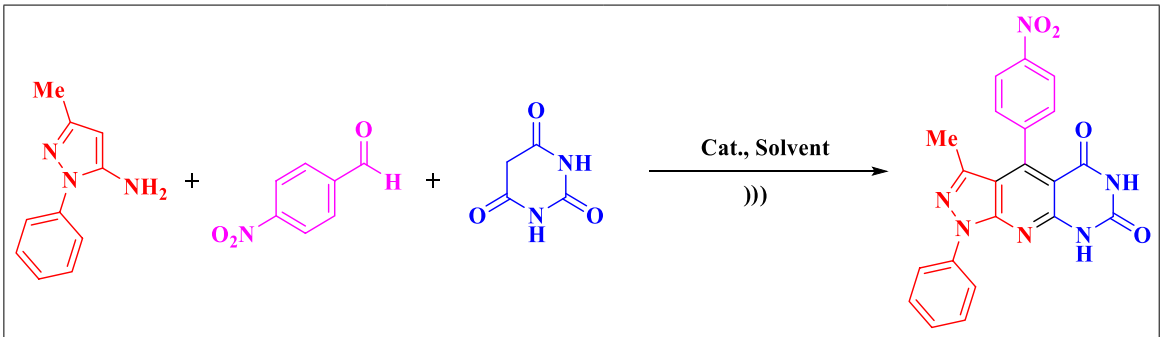

Entry	Solvent	Cat. (mg)	Sonication (min)	Yield (%)
1	DMF	–	120	Trace
2	DMF	5	75	25
3	DMF	7.5	60	45
4	DMF	10	50	72
5	DMF	15	50	72
6	H_2O	10	60	35
7	*n*-Hexane	10	60	25
8	EtOH	10	60	Trace
9	CH_2Cl_2	10	60	Trace
10	$CHCl_3$	10	60	28
11	EtOAc	10	60	46
12	CH_3CN	10	60	54
13	MeOH	10	60	Trace
14	–	10	60	15

Table 1. Effect of different amounts of catalysts and solvent (5 mL) in the synthesis of novel fused pyridines and 1,4-dihydropyridines with pyrazole and pyrimidine moieties by using the corresponding precursors under ultrasonic irradiation. Reaction conditions: 3-methyl-1-phenyl-1*H*-pyrazole-5-amine (1.0 mmol, 0.174 g), pyrimidine-2,4,6(1*H*,3*H*,5*H*)-trione (1.0 mmol, 0.128 g) and 4-nitrobenzaldehyde (1.0 mmol, 0.151 g).

nanomagnetic metal–organic frameworks (NMMOFs) catalyst was separated by an external magnet, washed with DMF and dried. The results indicated that the catalyst could be utilized for nine runs without any significant loss of its initial catalytic activity, which can be ascribed to the high stability of the synthesized catalyst (Fig. 8). Then, the reused catalyst was also characterized by FT-IR spectrum (Figure S6 see supporting information), N_2 adsorption–desorption isotherm (BET) and scanning electron microscope (SEM) images. The obtained spectra are as same as the corresponding spectra of fresh catalyst (Figures S7, S8 see supporting information), Furthermore, to compare the performance of nanomagnetic metal–organic frameworks (NMMOFs) catalyst for the synthesis of desired fused pyridines and 1,4-dihydropyridines with pyrazole and pyrimidine moieties via a cooperative vinylogous anomeric based oxidation, we have used various organic and inorganic acid catalysts for condensation reaction between 4-nitro benzaldehyde (1.0 mmol, 0.151 g), 3-methyl-1-phenyl-1*H*-pyrazole-5-amine (1.0 mmol, 0.174 g) and pyrimidine-2,4,6(1*H*,3*H*,5*H*)-trione (1.0 mmol, 0.128 g). As Table 3 indicates, Fe_3O_4@Co(BDC)-NH_2 is the best of choice for the synthesis of pyrazolo[4′,3′:5,6]pyrido[2,3-*d*]pyrimidine-5,7(6*H*)-dione (Table 3).

Conclusion

In summary, a novel core–shell nanomagnetic metal–organic frameworks Fe_3O_4@Co(BDC)-NH_2 as a new catalyst was prepared and fully characterized. This catalyst was applied for the synthesis of a range of novel fused pyridines and 1,4-dihydropyridines with pyrazole and pyrimidine moieties with good yields via a cooperative vinylogous anomeric based oxidation mechanism under ultrasonic irradiation. The obtained biological-based compounds are suitable candidates for biological studies. The described catalyst is reusable and easily separated by an external magnet.

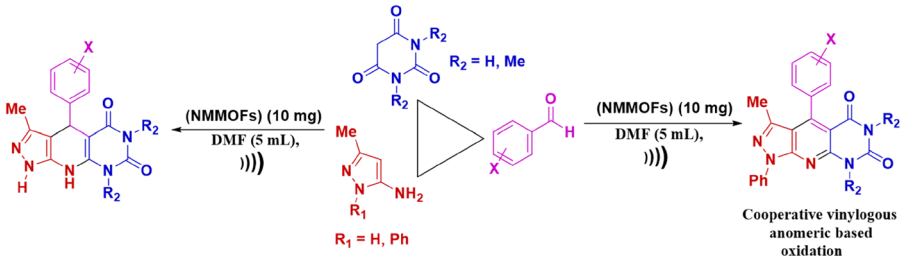

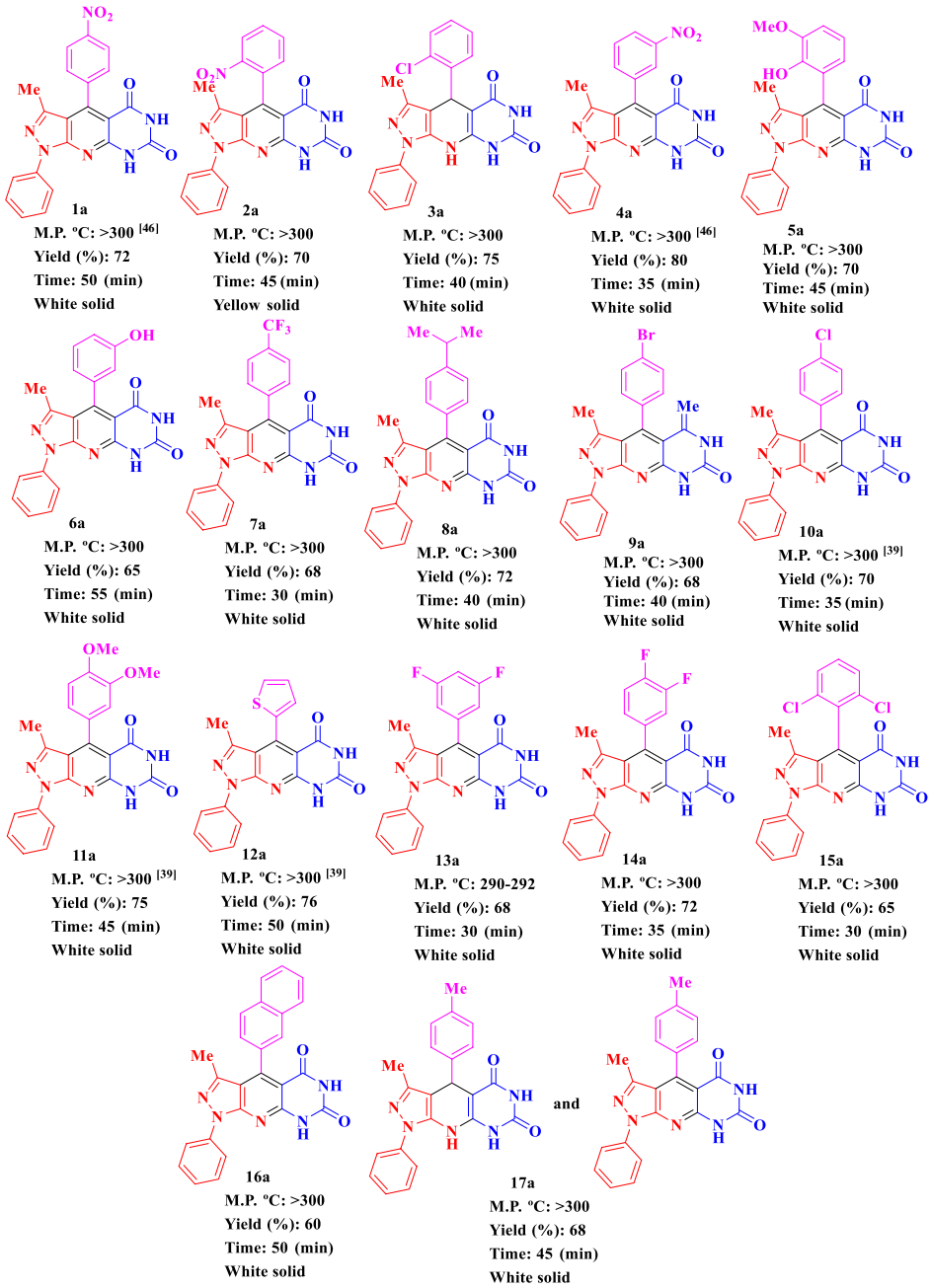

1a
M.P. °C: >300 [46]
Yield (%): 72
Time: 50 (min)
White solid

2a
M.P. °C: >300
Yield (%): 70
Time: 45 (min)
Yellow solid

3a
M.P. °C: >300
Yield (%): 75
Time: 40 (min)
White solid

4a
M.P. °C: >300 [46]
Yield (%): 80
Time: 35 (min)
White solid

5a
M.P. °C: >300
Yield (%): 70
Time: 45 (min)
White solid

6a
M.P. °C: >300
Yield (%): 65
Time: 55 (min)
White solid

7a
M.P. °C: >300
Yield (%): 68
Time: 30 (min)
White solid

8a
M.P. °C: >300
Yield (%): 72
Time: 40 (min)
White solid

9a
M.P. °C: >300
Yield (%): 68
Time: 40 (min)
White solid

10a
M.P. °C: >300 [39]
Yield (%): 70
Time: 35 (min)
White solid

11a
M.P. °C: >300 [39]
Yield (%): 75
Time: 45 (min)
White solid

12a
M.P. °C: >300 [39]
Yield (%): 76
Time: 50 (min)
White solid

13a
M.P. °C: 290-292
Yield (%): 68
Time: 30 (min)
White solid

14a
M.P. °C: >300
Yield (%): 72
Time: 35 (min)
White solid

15a
M.P. °C: >300
Yield (%): 65
Time: 30 (min)
White solid

16a
M.P. °C: >300
Yield (%): 60
Time: 50 (min)
White solid

and

17a
M.P. °C: >300
Yield (%): 68
Time: 45 (min)
White solid

Table 2. (continued)

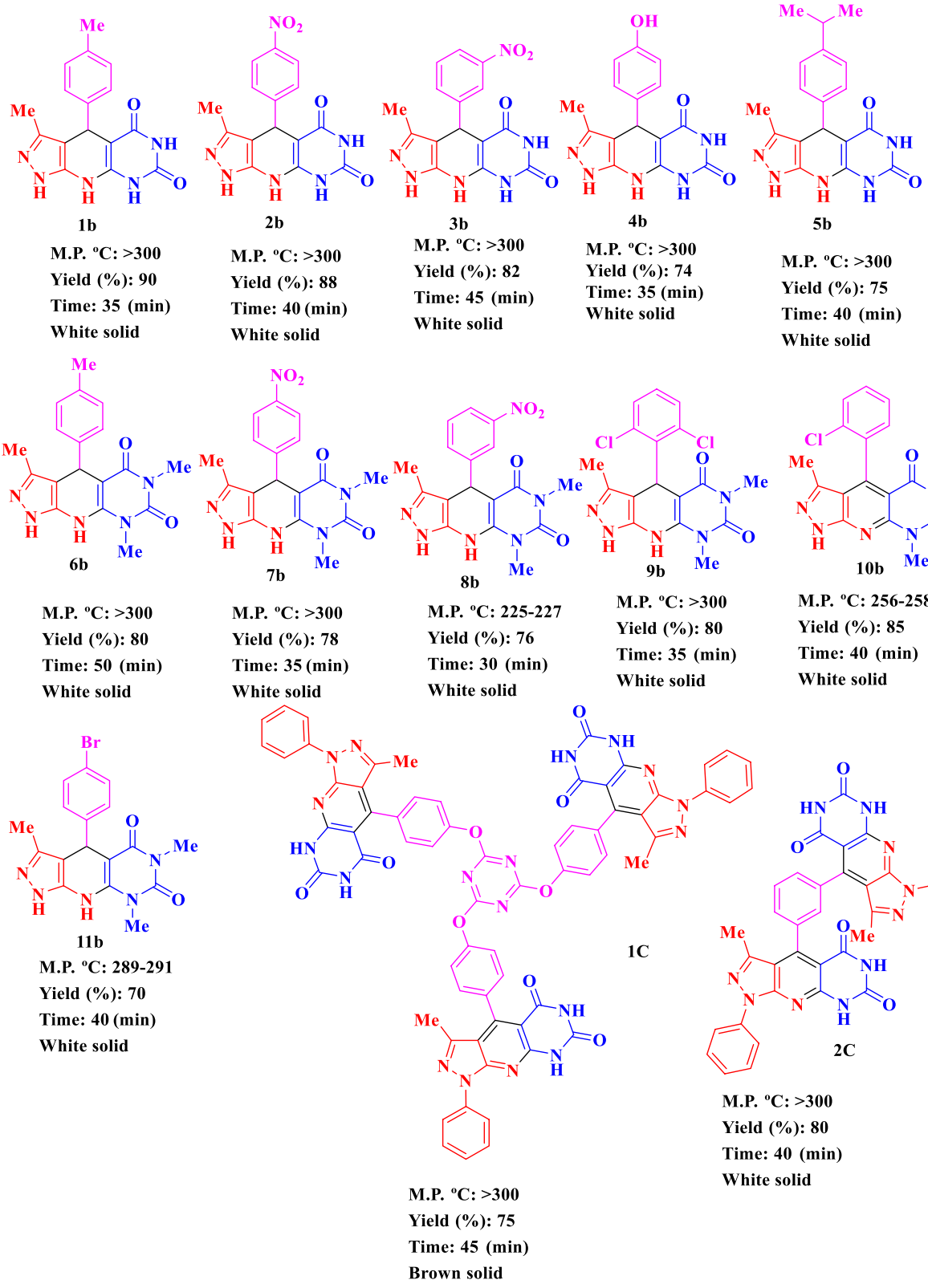

Table 2. Synthesis of (**a**) 3-methyl-1,4-diphenyl-1,8-dihydro-5*H*-pyrazolo[4′,3′:5,6]pyrido[2,3-*d*]pyrimidine-5,7(6*H*)-dione derivatives, (**b**) 3-Methyl-4-phenyl-1,4,8,9-tetrahydro-5*H*-pyrazolo[4′,3′:5,6]pyrido[2,3-*d*] pyrimidine-5,7(6*H*)-dione derivatives, (**c**) Bis and tris 3-methyl-1,4-diphenyl-1,8-dihydro-5*H*-pyrazolo[4′,3′:5,6] pyrido[2,3-*d*]pyrimidine-5,7(6*H*)-dione derivatives using Fe_3O_4@Co(BDC)-NH_2 under ultrasonic irradiation.

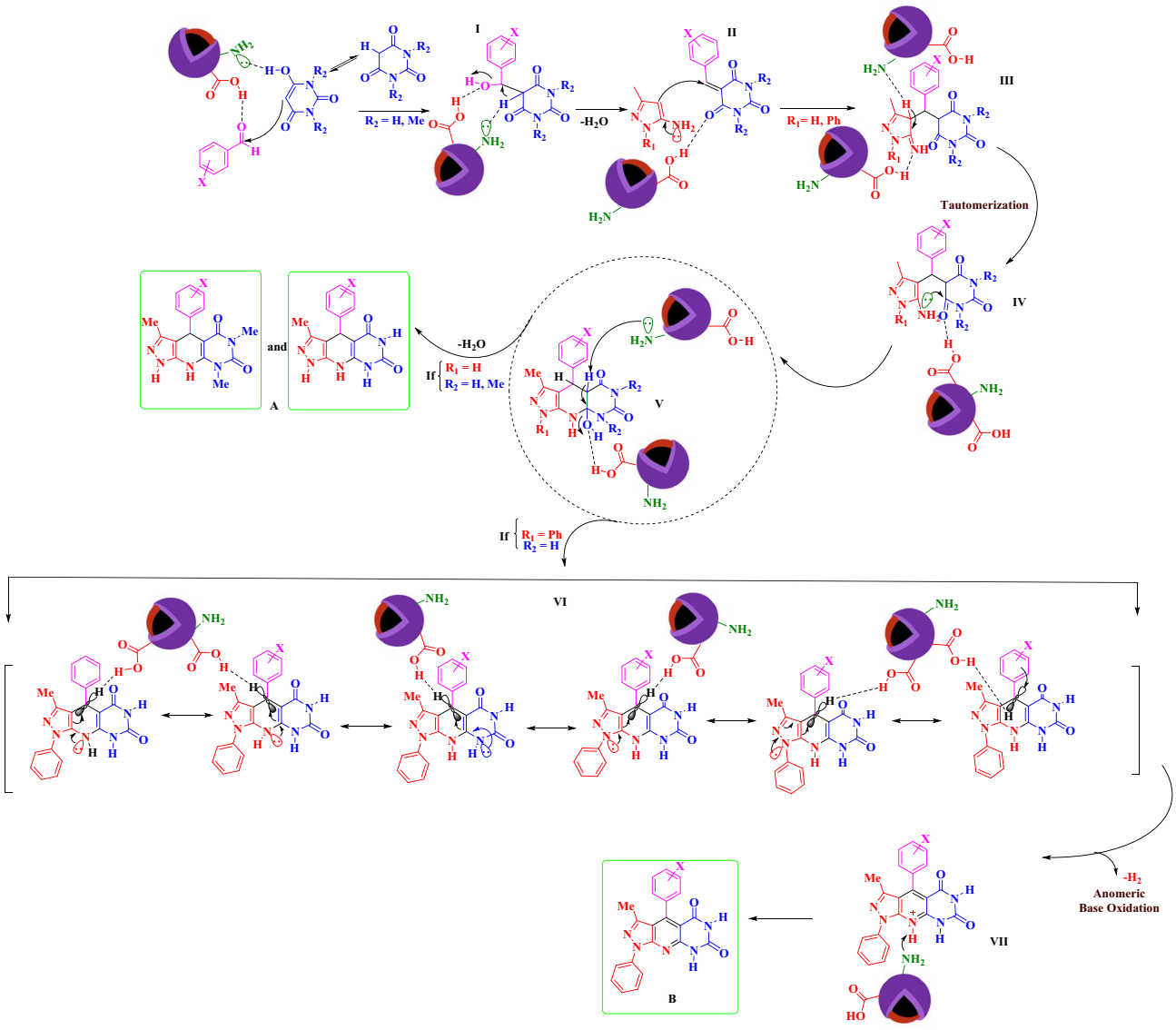

Scheme 3. Proposed mechanism for the preparation of novel fused pyridines and 1,4-dihydropyridines with pyrazole and pyrimidine moieties via a cooperative vinylogous anomeric based oxidation.

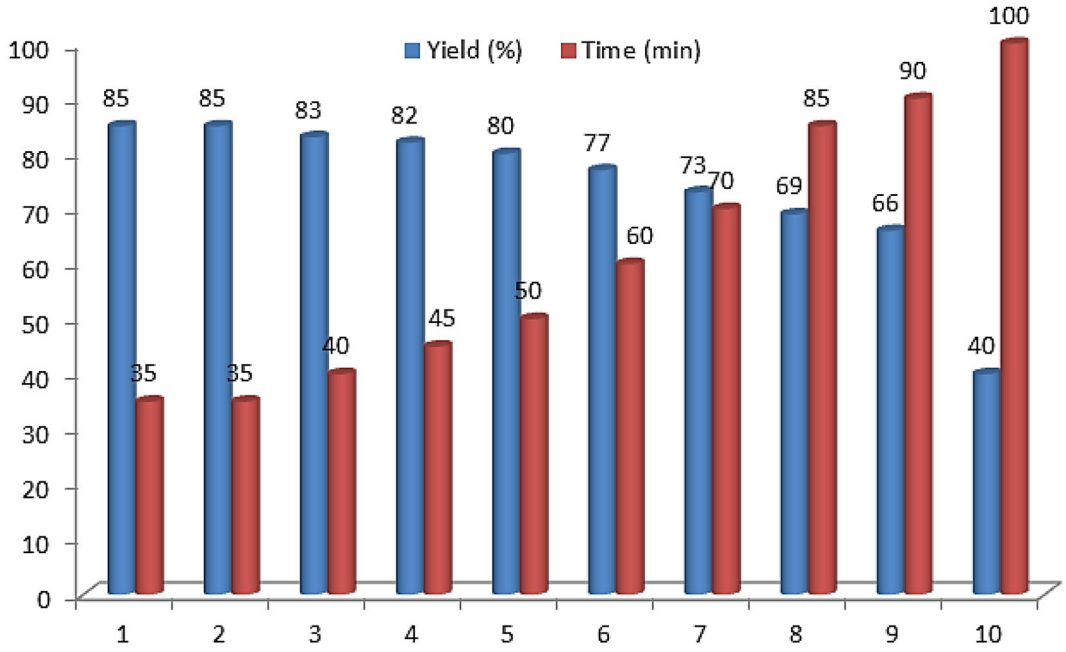

Figure 8. Recyclability of Fe_3O_4@Co(BDC)-NH_2 as a catalyst in the synthesis pyrazolo[4′,3′:5,6]pyrido[2,3-*d*] pyrimidine-5,7(6*H*)-dione.

Entry	Catalyst	(mol%)	Time (min)	Yield (%)
1	$FeCl_3$	10	120	25
2	[PVI-SO_3H]FeCl[56]	10	120	48
3	Fe_3O_4	10 mg	120	Trace
4	NH_4NO_3	10	120	Trace
5	SSA[57,58]	10 mg	120	35
6	Nano-SB-[PSIM]Cl[59]	10 mg	120	Trace
7	$NaHSO_4$	10	120	–
8	GTBSA[60]	10	120	55
9	SBA-15/$(CH_2)_3$ $N(CH_2PO_3H_2)_2$[61]	10 mg	120	35
10	[Py-SO_3H]Cl[62]	10	120	35
11	*p*-TSA	10	120	25
12	Et_3N	10	120	–
13	MIL-100(Cr)/NHEtN$(CH_2PO_3H_2)_2$[63]	10 mg	120	63
14	APVPB[64]	10 mg	120	40
15	MHMHPA[65]	10	120	55
16	GTMPA[66]	10	120	40
17	$Co(NO_3)_3{\cdot}6H_2O$	10	120	36
18	H_2BDC-NH_2	10	120	42
19	Fe_3O_4@Co(BDC)-NH_2	10 mg	50	72[a]

Table 3. Synthesis of pyrazolo[4′,3′:5,6]pyrido[2,3-d]pyrimidine-5,7(6*H*)-dionein the presence of various catalysts under ultrasonic irradiation. [a]This work.

Received: 20 August 2020; Accepted: 2 February 2021
Published online: 05 March 2021

References

1. Amaniampong, P. N. & Jerome, F. Catalysis under ultrasonic irradiation: A sound synergy. *Curr. Opin. Chem.* **22**, 7–12 (2020).
2. Amaro-Gahete, J. *et al.* Fast ultrasound-assisted synthesis of highly crystalline MIL-88A particles and their application as ethylene adsorbents. *Ultrason. Sonochem.* **50**, 59–66 (2019).
3. Bigdeli, F., Rouhani, F., Morsali, A. & Ramazani, A. Ultrasonic-assisted synthesis of the nanostructures of a Co(II) metal organic framework as a highly sensitive fluorescence probe of phenol derivatives. *Ultrason. Sonochem.* **62**, 104862 (2020).

4. Ke, F. *et al.* Facile fabrication of magnetic metal–organic framework nanocomposites for potential targeted drug delivery. *J. Mater. Chem.* **21**, 3843–3848 (2011).
5. Li, J. R., Kuppler, R. J. & Zhou, H. C. Selective gas adsorption and separation in metal–organic frameworks. *Chem. Soc. Rev.* **38**, 1477–1504 (2009).
6. Ricco, R., Malfatti, L., Takahashi, M., Hill, A. J. & Falcaro, P. Applications of magnetic metal–organic framework composites. *J. Mater. Chem. A* **1**, 13033–13045 (2013).
7. Hu, X. *et al.* Magnetic metal–organic frameworks containing abundant carboxylic groups for highly effective enrichment of glycopeptides in breast cancer serum. *Talanta* **204**, 446–454 (2019).
8. Rostamnia, S., Alamgholiloo, H. & Jafari, M. Ethylene diamine post-synthesis modification on open metal site Cr-MOF to access efficient bifunctional catalyst for the Hantzsch condensation reaction. *Appl. Organomet. Chem.* **32**, e4370 (2018).
9. Alamgholiloo, H., Rostamnia, S., Hassankhani, A. & Banaei, R. Synthesis of a zeoliticimidazolate-zinc metal–organic framework and the combination of its catalytic properties with 2, 2, 2-trifluoroethanol for *N*-formylation. *Synlett* **29**, 1593–1596 (2018).
10. Alamgholiloo, H. *et al.* Stepwise post-modification immobilization of palladium schiff-base complex on to the OMS-Cu (BDC) metal–organic framework for Mizoroki–Heck cross-coupling reaction. *Appl. Organomet. Chem.* **32**, e4539 (2018).
11. Rostamnia, S. & Jafari, M. Metal–organic framework of amine-MIL-53(Al) as active and reusable liquid-phase reaction inductor for multicomponent condensation of Ugi-type reactions. *Appl. Organomet. Chem.* **3**, 1–6 (2016).
12. Rostamnia, S. & Mohsenzad, F. Nanoarchitecturing of open metal site Cr-MOFs for oxodiperoxo molybdenum complexes $[MoO(O_2)_2$@En/MIL-100(Cr)] as promising and bifunctional catalyst for selective thioether oxidation. *Mol. Catal.* **445**, 12–20 (2018).
13. Hu, M. L. *et al.* Taking organic reactions over metal–organic frameworks as heterogeneous catalysis. *Microporous Mesoporous Mater.* **256**, 111–127 (2018).
14. Chen, M. N., Mo, L. P., Cui, Z. S. & Zhang, Z. H. Magnetic nanocatalysts: Synthesis and application in multicomponent reactions. *Curr. Opin. Chem.* **15**, 27–37 (2019).
15. Bai, S. *et al.* Magnetic biochar catalysts from anaerobic digested sludge: Production, application and environment impact. *Environ. Int.* **126**, 302–308 (2019).
16. Maleki, B., Reiser, O., Esmaeilnezhad, E. & Choi, H. J. SO_3H-dendrimer functionalized magnetic nanoparticles (Fe_3O_4@ $DNH(CH_2)_4SO_3H$): Synthesis, characterization and its application as a novel and heterogeneous catalyst for the one-pot synthesis of polyfunctionalizedpyrans and polyhydroquinolines. *Polyhedron* **162**, 129–141 (2019).
17. Koukabi, N. *et al.* A magnetic particle-supported sulfonic acid catalyst: Tuning catalytic activity between homogeneous and heterogeneous catalysis. *Adv. Synth. Catal.* **354**, 2001–2008 (2012).
18. Abu-Dief, A. M. & Abdel-Fatah, S. M. Development and functionalization of magnetic nanoparticles as powerful and green catalysts for organic synthesis. *Beni-Suef Univ. J. Basic Appl. Sci.* **7**, 55–67 (2018).
19. Yao, Y. *et al.* Magnetic recoverable $MnFe_2O_4$ and $MnFe_2O_4$-graphene hybrid as heterogeneous catalysts of peroxymonosulfate activation for efficient degradation of aqueous organic pollutants. *J. Hazard. Mater.* **270**, 61–70 (2014).
20. Lu, N., He, X., Wang, T., Liu, S. & Hou, X. Magnetic solid-phase extraction using MIL-101(Cr)-based composite combined with dispersive liquid-liquid microextraction based on solidification of a floating organic droplet for the determination of pyrethroids in environmental water and tea samples. *Microchem. J.* **137**, 449–455 (2018).
21. Gao, G., Di, J. Q., Zhang, H. Y., Mo, L. P. & Zhang, Z. H. A magnetic metal organic framework material as a highly efficient and recyclable catalyst for synthesis of cyclohexenone derivatives. *J. Catal.* https://doi.org/10.1016/j.jcat.2020.04.013 (2020).
22. Safari, M., Yamini, Y., Masoomi, M. Y. & Morsali, A. Magnetic metal–organic frameworks for the extraction of trace amounts of heavy metal ions prior to their determination by ICP-AES. *Microchim. Acta* **184**, 1555–1564 (2017).
23. Yamini, Y., Safari, M., Morsali, A. & Safarifard, V. Magnetic frame work composite as an efficient sorbent for magnetic solid-phase extraction of plasticizer compounds. *J. Chromatogr. A* **1570**, 38–46 (2018).
24. Zhang, X. *et al.* Thermal conversion of an Fe_3O_4@metal–organic framework: A new method for an efficient Fe-Co/nanoporous carbon microwave absorbing material. *Nanoscale* **7**, 12932–12942 (2015).
25. Huo, J. B. *et al.* Direct epitaxial synthesis of magnetic Fe_3O_4@UiO-66 composite for efficient removal of arsenate from water. *Microporous Mesoporous Mater.* **276**, 68–75 (2019).
26. Fan, L. *et al.* Fe-MOF derived jujube pit like Fe_3O_4/C composite as sulfur host for lithium-sulfur battery. *Electrochim. Acta* **295**, 444–451 (2019).
27. Gao, Y., Liu, G., Gao, M., Huang, X. & Xu, D. Recent advances and applications of magnetic metal–organic frameworks in adsorption and enrichment removal of food and environmental pollutants. *Crit. Rev. Anal. Chem.* https://doi.org/10.1080/10408347.2019.1653166 (2019).
28. Nadar, S. S. & Rathod, V. K. Magnetic-metal organic framework (magnetic-MOF): A novel platform for enzyme immobilization and nanozyme applications. *Int. J. Biol. Macromol.* **120**, 2293–2302 (2018).
29. Wang, R., Zhang, C., Wang, S. & Zhou, Y. Synthesis and application of magnetic metal–organic frameworks. *Prog. Chem.* **27**, 945–952 (2015).
30. Grivsky, E. M., Lee, S., Sigel, C. W., Duch, D. S. & Nichol, C. A. Synthesis and antitumor activity of 2, 4-diamino-6-(2,5-dimethoxybenzyl)-5-methylpyrido [2,3-*d*] pyrimidine. *J. Med. Chem.* **23**, 327–329 (1980).
31. Deb, M. L. & Bhuyan, P. J. Synthesis of novel classes of pyrido[2,3-*d*]-pyrimidines, Pyrano[2,3-*d*]pyrimidines, and pteridines. *Synth. Commun.* **36**, 3085–3090 (2006).
32. Devi, I., Borah, H. N. & Bhuyan, P. J. Studies on uracils: A facile one-pot synthesis of oxazino[4,5-*d*]$^-$, pyrano[2,3-*d*]$^-$, pyrido[2,3-*d*]$^-$ and pyrimido[4,5-*d*] pyrimidines using microwave irradiation in the solid state. *Tetrahedron Lett.* **45**, 2405–2408 (2004).
33. Lee, H. M., Chiu, P. L., Hu, C. H., Lai, C. L. & Chou, Y. C. Synthesis and structural characterization of metal complexes based on pyrazole/imidazolium chlorides. *J. Organomet. Chem.* **690**, 403–414 (2005).
34. Allais, C., Grassot, J. M., Rodriguez, J. & Constantieux, T. Metal-free multicomponent synthesis of pyridines. *Chem. Rev.* **114**, 10829–10868 (2014).
35. Tabacchi, G., Vanoni, M. A., Gamba, A. & Fois, E. Does negative hyperconjugation assist enzymatic dehydrogenations. *Chem. Phys. Chem.* **8**, 1283–1288 (2007).
36. Hamasaka, G., Tsuji, H. & Uozumi, Y. Organoborane-catalyzed hydrogenation of unactivated aldehydes with a Hantzsch ester as a synthetic NAD(P)H analogue. *Synlett* **26**, 2037–2041 (2015).
37. He, T. *et al.* Base-promoted cascade approach for the preparation of reduced knoevenagel adducts using hantzsch esters as reducing agent in water. *Synlett* **27**, 1864–1869 (2016).
38. Bai, C. B., Wang, N. X., Xing, Y. & Lan, X. W. Progress on chiral NAD(P)H model compounds. *Synlett* **13**, 402–414 (2017).
39. Zhao, X., Xiao, J. & Tang, W. Enantioselective reduction of 3-substituted quinolines with a cyclopentadiene-based chiral Brønsted acid. *Synthesis* **49**, 3157–3164 (2017).
40. Moradi, S. *et al.* An efficient catalytic method for the synthesis of pyrido[2,3-*d*] pyrimidines as biologically drug candidates by using novel magnetic nanoparticles as a reusable catalyst. *Appl. Organomet. Chem.* **32**, e4043 (2017).
41. Rajabi-Salek, M., Zolfigol, M. A. & Zarei, M. Synthesis of a novel DABCO-based nanomagnetic catalyst with sulfonic acid tags: Application to the synthesis of diverse spiropyrans. *Res. Chem. Intermed.* **44**, 5255–5269 (2018).
42. Zhang, Y. *et al.* Tunable chiral metal organic frameworks toward visible light-driven asymmetric catalysis. *Sci. Adv.* **3**(8), e1701162 (2017).

43. Yang, Y. *et al.* Synthesis and characterization of three amino-functionalized metal–organic frameworks based on the 2-aminoterephthalic ligand. *Dalton Trans.* **44**, 8190–8197 (2015).
44. Li, C. *et al.* Mesoporous nanostructured Co_3O_4 derived from MOF template: A high-performance anode material for lithium-ion batteries. *J. Mater. Chem.* **3**, 5585–5591 (2015).
45. Bhamini, B., Shanmugam, S. A. & Tan, M. Study of aluminium doped transition metal ferrite nanomaterials as supercapacitor electrodes. *J. Eng. Res.* **2**, 1–10 (2014).
46. Shi, F. *et al.* Pot atom and step economic synthesis of fused three heterocyclic ring compounds under microwave irradiation in water. *J. Heterocycl. Chem.* **45**, 1305–1310 (2008).
47. Yarie, M. Catalytic anomeric based oxidation. *Iran. J. Catal.* **7**, 85–88 (2017).
48. Yarie, M. Catalytic vinylogous anomeric based oxidation. *Iran. J. Catal.* **10**, 79–83 (2020).
49. Babaee, S., Zolfigol, M. A., Zarei, M. & Zamanian, J. 1,10-Phenanthroline-based molten salt as a bifunctionalsulfonic acid catalyst: Application to the synthesis of *N*-heterocyclecompounds via anomericbased oxidation. *ChemistrySelect* **3**, 8947–8954 (2018).
50. Babaee, S., Zarei, M., Sepehrmansourie, H., Zolfigol, M. A. & Rostamnia, S. Synthesis of metal–organic frameworks MIL-101(Cr)-NH_2 containing phosphorous acid functional groups: Application for the synthesis of *N*-amino-2-pyridone and pyrano [2,3-*c*] pyrazole derivatives *via* a cooperative vinylogous anomeric based oxidation. *ACS Omega* **5**, 6240–6249 (2020).
51. Ghasemi, P., Yarie, M., Zolfigol, M. A., Taherpour, A. A. & Torabi, M. Ionically tagged magnetic nanoparticles with urea linkers: Application for preparation of 2-aryl-quinoline-4-carboxylic acids via an anomeric-based oxidation mechanism. *ACS Omega* **5**, 3207–3217 (2020).
52. Karimi, F., Yarie, M. & Zolfigol, M. A. A convenient method for synthesis of terpyridines via a cooperative vinylogous anomeric based oxidation. *RSC Adv.* **10**, 25828–25835 (2020).
53. Karimi, F., Yarie, M. & Zolfigol, M. A. Synthesis and characterization of Fe_3O_4@SiO_2@$(CH_2)_3NH(CH_2)_2O_2P(OH)_2$ and its catalytic application in the synthesis of benzo-[h]quinoline-4-carboxylic acids via a cooperative anomeric based oxidation mechanism. *Mol. Catal.* **489**, 110924 (2020).
54. Karimi, F., Yarie, M. & Zolfigol, M. A. Fe_3O_4@SiO_2@$(CH_2)_3$-urea-thiourea: A novel hydrogen-bonding and reusable catalyst for the construction of bipyridine-5-carbonitriles *via* a cooperative vinylogous anomeric based oxidation. *Mol. Catal.* **489**, 111201 (2020).
55. Dashteh, M. *et al.* Synthesis of cobalt tetra-2,3-pyridiniumporphyrazinato with sulfonic acid tags as an efficient catalyst and its application for the synthesis of bicyclic ortho-aminocarbonitriles, cyclohexa-1,3-dienamines and 2-amino-3-cyanopyridines. *RSC Adv.* **10**, 27824–27834 (2020).
56. Sepehrmansourie, H., Zarei, M., Taghavi, R. & Zolfigol, M. A. Mesoporous ionically tagged cross-linked poly (vinyl imidazole) s as novel and reusable catalysts for the preparation of *N*-heterocycle spiropyran. *ACS Omega* **4**, 17379–17392 (2019).
57. Zolfigol, M. A. Silica sulfuric acid/$NaNO_2$ as a novel heterogeneous system for production of thionitrites and disulfides under mild conditions. *Tetrahedron* **57**, 9509–9511 (2001).
58. Sepehrmansourie, H. Silica sulfuric acid (SSA): As a multipurpose catalyst. *Iran. J. Catal.* **10**, 175–179 (2020).
59. Zare, A. *et al.* Design and characterization of nano-silica-bonded 3-n-propyl-1-sulfonic acid imidazolium chloride nano-SB-[PSIM] Cl as a novel, heterogeneous and reusable catalyst for the condensation of arylaldehydes with β-naphthol and alkyl carbamates. *Res. Chem. Intermed.* **42**, 2365–2378 (2016).
60. Zarei, M., Sepehrmansourie, H., Zolfigol, M. A., Karamian, R. & Moazzami Farida, S. H. Novel nano-size and crab-like biological-based glycoluril with sulfonic acid tags as a reusable catalyst: Its application to the synthesis of new mono- and bis-spiropyrans and their in vitro biological studies. *New. J. Chem.* **42**, 14308–14317 (2018).
61. Jalili, F., Zarei, M., Zolfigol, M. A., Rostamnia, S. & Moosavi-Zare, A. R. SBA-15/PrN$(CH_2PO_3H_2)_2$ as a novel and efficient mesoporous solid acid catalyst with phosphorous acid tags and its application on the synthesis of new pyrimido[4,5-*b*]quinolones and pyrido[2,3-*d*]pyrimidines via anomeric based oxidation. *Microporous Mesoporous Mater.* **294**, 109865 (2020).
62. Moosavi-Zare, A. R., Zolfigol, M. A., Zarei, M., Khakyzadeh, V. & Hasaninejad, A. Design, characterization and application of new ionic liquid 1-sulfopyridinium chloride as an efficient catalyst for tandem Knoevenagel-Michael reaction of 3-methyl-1-phenyl-1*H*-pyrazol-5(4*H*)-one with aldehydes. *Appl. Catal. A Gen.* **467**, 61–68 (2013).
63. Sepehrmansourie, H. *et al.* Multilinker phosphorous acid anchored En/MIL-100 (Cr) as a novel nanoporous catalyst for the synthesis of new *N*-heterocyclic pyrimido [4, 5-*b*] quinolones. *Mol. Catal.* **481**, 110303 (2020).
64. Noroozizadeh, E. *et al.* Synthesis of bis-coumarins over acetic acid functionalized poly(4-vinylpyridinum) bromide (APVPB) as a green efficient catalyst under solvent-free conditions their biological activity. *J. Iran. Chem. Soc.* **15**, 471–481 (2018).
65. Afsar, J. *et al.* Synthesis and application of melamine-based nano catalyst with phosphonic acid tags in the synthesis of (3′-indolyl) pyrazolo[3,4-*b*]pyridines via vinylogous anomeric based oxidation. *Mol. Catal.* **482**, 110666 (2020).
66. Moradi, S., Zolfigol, M. A., Zarei, M., Alonso, D. A. & Khoshnood, A. Synthesis of a biological-based glycoluril with phosphorous acid tags as a new nanostructured catalyst: Application for the synthesis of novel natural henna-based compounds. *ChemistrySelect* **3**, 3042–3047 (2018).

Acknowledgements

We thank the Bu-Ali Sina University and Iran National Science Foundation (INSF) (Grant Number: 98001912) for financial support.

Author contributions

H.S., M.Z. and S.B.: methodology, validation, investigation, writing the original draft. M.A.Z.: supervision, resources, project administration, funding acquisition, conceptualization, writing—review and editing. S.R.: advisor of project and editing of the manuscript.

Competing interests

The authors declare no competing interests.

Additional information

Supplementary Information The online version contains supplementary material available at https://doi.org/10.1038/s41598-021-84005-2.

Correspondence and requests for materials should be addressed to M.Z., M.A.Z. or S.R.

Reprints and permissions information is available at www.nature.com/reprints.

Publisher's note Springer Nature remains neutral with regard to jurisdictional claims in published maps and institutional affiliations.